JCTC Journal of Chemical Theory and Computation

pubs.acs.org/JCTC Article

Spin-Density Functional Regularization for Singlet Diradicals

Yi Shi, Yuming Shi, Adam Wasserman,* and Xin-Zheng Li*

Cite This: J. Chem. Theory Comput. 2025, 21, 8420−8433 Read Online

ACCESS | Metrics & More | Article Recommendations | Supporting Information

ABSTRACT: Broken-symmetry density functional theory (DFT) is one of the commonly used methods for treating the static-correlation effects in singlet diradicals, which arise from the (quasi-)degeneracy of their frontier orbitals. Although the method yields quantitatively accurate energies for simple cases, such as stretched diatomic molecules, it fails for other systems with more complicated electronic structures due to the artificially broken spin symmetries. In this work, we present a spin-density functional regularization (SR) approach within the framework of partition density functional theory (PDFT) to correct errors arising from artificial symmetry breaking in broken-symmetry DFT calculations. To demonstrate the efficacy of our method, we examine the automerization of cyclobutadiene, a classic example where the transition state is a singlet diradical. While conventional broken-symmetry DFT calculations using standard exchange−correlation density functional approximations systematically underestimate the energy of the automerization transition state, SR-PDFT effectively eliminates the influences of artificial symmetry breaking and yields chemically accurate barrier heights for the reaction.

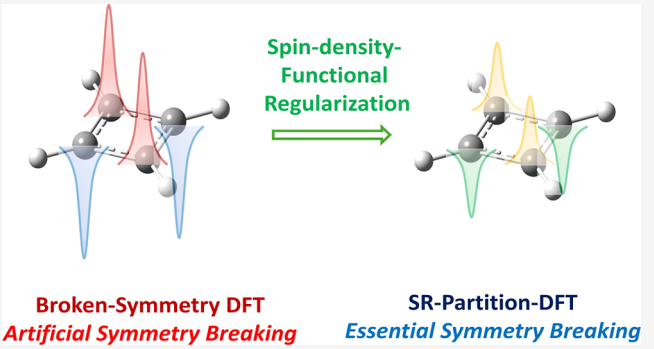

1. INTRODUCTION

Diradicals are open-shell molecular systems with two quasi-degenerate frontier orbitals that are singly occupied by two unpaired electrons. The low-lying spin states of these unpaired electrons govern a broad range of interesting chemical processes. For example, the energy gap between the lowest-lying singlet and triplet states (S-T gap) determines the effective exchange coupling in molecular magnets[1] and the efficiency of organic light-emitting diodes.[2,3] The singlet state also has a central role in heavy-atom quantum tunneling,[4−6] e.g., the π-bond shifting in antiaromatic annulenes.[7−11] A quantitative description of the singlet state of diradicals represents a great challenge for theoretical chemistry, because the static electron correlation arising from (quasi-)degenerate frontier orbitals typically requires a multireference treatment.[12,13] The complete active space self-consistent field (CASSCF)[14−16] is a representative multireference method and inherently includes static correlation, but it does not properly take into account the effect of dynamic correlation.[17] Dynamic correlation must be incorporated either by adding a second-order perturbation to the CASSCF wave function (CASPT2)[17,18] or through the more expensive multireference configuration interaction (MRCI) scheme.[19]

A simpler treatment of singlet diradicals comes from the spin-unrestricted formulation of Kohn−Sham density functional theory (KS-DFT). When spin-unrestricted calculations yield spin-densities that have lower symmetries than the true ground-state wave function of the system, this approach is termed broken-symmetry DFT.[20,21] If the exact exchange−correlation (XC) functional were used in KS-DFT, symmetry breaking would be unnecessary since the exact functional inherently captures all electron correlations and gives the correct ground-state energy. However, practical calculations rely on approximate density functional approximations (DFAs). While spin-restricted DFT (RDFT, where $n_\uparrow(\boldsymbol{r}) = n_\downarrow(\boldsymbol{r})$) typically performs well for weakly correlated systems, it often significantly overestimates the energies of strongly correlated systems with (nearly) degenerate frontier orbitals.[22] This degeneracy of orbitals can be removed by broken-symmetry DFT, since it employs separate sets of spatial orbitals for spin-up and spin-down electrons.[23,24]

Despite its explicit breaking of spin symmetry, broken-symmetry DFT yields quantitatively accurate energies for numerous strongly correlated systems, including some simple singlet diradicals.[25,26] The reason is elucidated by Perdew et al.: the symmetry-broken wave function (or spin-densities) in approximate broken-symmetry DFT represents a snapshot of the electron correlation embodied in the exact symmetry-unbroken ground-state wave function.[27] For finite systems like molecules, the strong electron correlations that appear as fluctuations in their ground states are not observable in the

Received: June 9, 2025
Revised: August 14, 2025
Accepted: August 18, 2025
Published: August 22, 2025



Downloaded from pubs.acs.org/jctcce/article-pdf/21/17/8420/4126030/ct5c00942.pdf by PEKING UNIV user on 04 November 2026

© 2025 American Chemical Society

https://doi.org/10.1021/acs.jctc.5c00942
J. Chem. Theory Comput. 2025, 21, 8420−8433

(exact) static symmetry-unbroken wave functions, whereas they are "frozen" in the snapshot revealed by the broken-symmetry solution. The information on those fluctuations is not available from RDFT because this method presents an average of the electron correlation in the system. The use of DFAs in RDFT makes this average deviate from the true correlation. On the other hand, the broken-symmetry DFT solution often yields correct energies, though it only represents a "cross-section" of the true electron correlation.

Unfortunately, broken-symmetry DFT does not always yield quantitatively correct energies for singlet diradicals, especially for molecules with complicated electronic structures.[25,26,28] The unphysically broken spin symmetries, also known as spin contamination, is not a significant issue for triplet states as their energies can be evaluated from a single-determinantal wave function, but it can result in substantial errors for open-shell singlet systems. Several spin-decontamination procedures have been proposed, such as the approximate spin-projection correction[29] and fractional-spin DFT.[30,31] Wave functions in these spin-decontaminated methods are proper spin eigenfunctions and provide satisfactory results for some singlet diradicals. One example where those spin-decontamination schemes do not work is the automerization of cyclobutadiene (CBD),[32] which is a special case of the aforementioned π-bond shifting of annulenes. Previous theoretical investigations suggest that the transition state of this automerization is a singlet diradical with a square geometry.[33,34] An accurate estimation of the automerization barrier height has been considered a challenging task even for the state-of-the-art multireference methods.[9,34−47] In terms of broken-symmetry DFT, several commonly used DFAs have been reported to significantly underestimate this barrier height.[35,48] Neither the approximate spin-projection correction nor fractional-spin DFT leads to meaningful improvements.[31,35] The spin contamination leads to a symmetry-broken wave function that does not appropriately reflect the realistic electron correlation embodied by the correct wave function of the transition state. In other words, a biased incorrect evaluation of spin polarization appears in the solution of broken-symmetry DFT and causes an unphysical lowering of the total energy.

In the present work, rather than attempting to remove the spin contamination from broken-symmetry DFT (i.e., we do not intend to obtain the spin-unpolarized open-shell singlet state), we exploit a distinction between *essentail* and *artificial* symmetry breaking, as suggested by Lee et al.[49−51] The symmetry breaking is essential when it fully accounts for the static electron correlation exhibited by the system of interest. In contrast, artificial symmetry breaking introduces excessive spin polarization in the broken-symmetry state and leads to an unphysical underestimation of electronic energies.

Herein, we employ a partitioning-based formulation of DFT, partition density functional theory (PDFT),[52−54] as a prescription for the inappropriate symmetry breaking in the broken-symmetry DFT solution. PDFT is well suited to address the problem because the real-space partitioning allows for the design of unique approximations to modulate local spin polarization within the molecule. Starting from a broken-symmetry DFT calculation done with a given DFA, a spin-density-functional regularization (SR) procedure is incorporated into the PDFT workflow to correct the error arising from artificial symmetry breaking of spin-densities. The procedure necessitates the knowledge of spin polarization in an ideal broken-symmetry state that breaks only the symmetries that are considered essential. We demonstrate that a SR-based correction to the nonadditive XC energy in PDFT can provide a quantitatively correct estimate of the automerization barrier of CBD when semilocal functionals are used as DFAs.

This article is structured as follows: Section 2 begins with an overview of the electronic structure of diradicals, followed by a review of the fundamental theories underlying broken-symmetry DFT and PDFT. We then discuss the introduction of the SR procedure and elucidate its role in eliminating the effects of artificial symmetry breaking. Section 3 details the computational methodology, including the implementation of SR-PDFT. In Section 4, we first present the automerization barrier heights of CBD calculated using six widely used DFAs within broken-symmetry DFT and compare them with results from state-of-the-art multireference methods. Subsequently, we demonstrate how SR-PDFT calculations improve upon the original broken-symmetry DFT results. Finally, Section 5 summarizes the advantages and limitations of SR-PDFT and discusses potential applications.

2. THEORETICAL BACKGROUND

This section is an overview of the theoretical methods involved in the present work. First, we illustrate the particularity of the electronic structure of diradicals and explain why it poses a challenge for many advanced quantum chemical methods. Next, we review the fundamental idea of broken-symmetry DFT and discuss the difficulties encountered in its application to singlet diradicals. Finally, we introduce the formalism of SR-PDFT, which is well suited to address these difficulties.

2.1. Electronic Structure of Diradicals. The electronic structure of diradicals is characterized by two unpaired electrons in two (nearly) degenerate molecular orbitals. We denote the degenerate orbitals as ψ_a and ψ_b. When the orbitals are singly occupied, there exist four ways of populating them with two electrons, as illustrated in Figure 1. Configurations

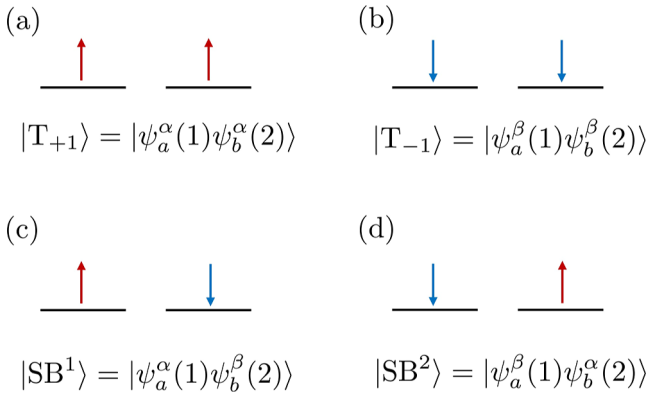

Figure 1. Possible electronic configurations of the two-orbital model given that orbitals are singly occupied. Each Dirac ket represents a single Slater determinant and α/β specifies the spin state (up/down) of a certain orbital.

(a) and (b) correspond to two triplet eigenstates $|T_{\pm1}\rangle$ of a model two-level Hamiltonian, where the subscript labels the spin magnetic quantum number M_s. The other two configurations, (c) and (d), are associated with two symmetry-broken states ($|SB^1\rangle$ and $|SB^2\rangle$) that are not eigenstates of the Hamiltonian, but their linear combinations give an open-shell singlet $|S_0^{OS}\rangle$ and a third triplet state $|T_0\rangle$

https://doi.org/10.1021/acs.jctc.5c00942
J. Chem. Theory Comput. 2025, 21, 8420−8433

Downloaded from pubs.acs.org/jctcce/article-pdf/21/17/8420/4126030/ct5c00942.pdf by PEKING UNIV user on 04 November 2026

$$
\begin{aligned}
|T_{+1}\rangle &= \frac{1}{\sqrt{2}}[\psi_a(1)\psi_b(2) - \psi_b(1)\psi_a(2)]\alpha(1)\alpha(2),\\
|T_{-1}\rangle &= \frac{1}{\sqrt{2}}[\psi_a(1)\psi_b(2) - \psi_b(1)\psi_a(2)]\beta(1)\beta(2),\\
|T_0\rangle &= \frac{1}{\sqrt{2(1+S_{12})}}(|SB^1\rangle + |SB^2\rangle)\\
&= \frac{1}{2\sqrt{(1-S_{ab}^2)}}[\psi_a(1)\psi_b(2) - \psi_b(1)\psi_a(2)]\\
&\quad [\alpha(1)\beta(2) + \beta(1)\alpha(2)],\\
|S_0^{OS}\rangle &= \frac{1}{\sqrt{2(1-S_{12})}}(|SB^1\rangle - |SB^2\rangle)\\
&= \frac{1}{2\sqrt{(1+S_{ab}^2)}}[\psi_a(1)\psi_b(2) + \psi_b(1)\psi_a(2)]\\
&\quad [\alpha(1)\beta(2) - \beta(1)\alpha(2)],
\end{aligned}
\tag{1}
$$

where $S_{12} = \langle SB^1|SB^2\rangle$ is the overlap integral between the symmetry-broken states $|SB^1\rangle$ and $|SB^2\rangle$. Note that $S_{12} = -S_{ab}^2 = -|\langle\psi_a|\psi_b\rangle|^2$ for the two-orbital model. The Hamiltonian of the two-orbital model

$$
H(1,2) = h(1) + h(2) + \frac{1}{r_{12}} \tag{2}
$$

includes one-body terms $h(1)$ and $h(2)$ representing the kinetic energy and the external potential for electrons 1 and 2, and a two-body term standing for the electron−electron interaction. It is then straightforward to derive the total energy expressions for the singlet and triplet eigenstates

$$
\begin{aligned}
E_S &= \frac{1}{1+S_{ab}^2}(h_a + h_b + J_{ab} + K_{ab} + 2h_{ab}S_{ab})\\
E_T &= \frac{1}{1-S_{ab}^2}(h_a + h_b + J_{ab} - K_{ab} - 2h_{ab}S_{ab})
\end{aligned}
\tag{3}
$$

where $h_a = \langle\psi_a|h(i)|\psi_a\rangle$, $h_b = \langle\psi_b|h(i)|\psi_b\rangle$, and $h_{ab} = \langle\psi_a|h(i)|\psi_b\rangle$ $(i = 1, 2)$ are matrix elements of the one-body operators in eq 2, and J_{ab} and K_{ab} stand for the Coulomb and exchange integrals between ψ_a and ψ_b, respectively. Generally, diradicals are classified into two categories, i.e., the so-called "joint" and "disjoint" diradicals.[12,13] The singly occupied orbitals ψ_a and ψ_b of disjoint diradicals are localized on different subsets of atoms, which implies a small or vanishing overlap integral S_{ab}. Under such a circumstance ($S_{ab} \to 0$), one may conclude from eq 3 that the S−T gap reduces to twice the magnitude of K_{ab}, i.e., $\Delta E_{ST} = E_S - E_T = 2K_{ab}$. Since K_{ab} depends on the magnitude of S_{ab} and is always non-negative, the two-orbital model predicts small but positive (or vanishing) S−T gaps for disjoint diradicals. On the other hand, joint diradicals possess orbitals that are distributed on the same atomic sites and manifest non-negligible S_{ab}. Consequently, the magnitudes of K_{ab} and h_{ab} for joint diradicals are considerably greater, and thus lead to relatively larger S−T gaps. So far, the difference between the two categories of diradicals has been rationalized by the interpretation from the two-orbital model.

Nevertheless, there exist some well-known examples of disjoint diradicals exhibiting negative S-T gaps.[12] For instance, the square CBD mentioned in Section 1 is such a case. Figure 2a shows CBD's ground-state and first-excited-state potential energy surfaces (PESs). The ground-state surface has a

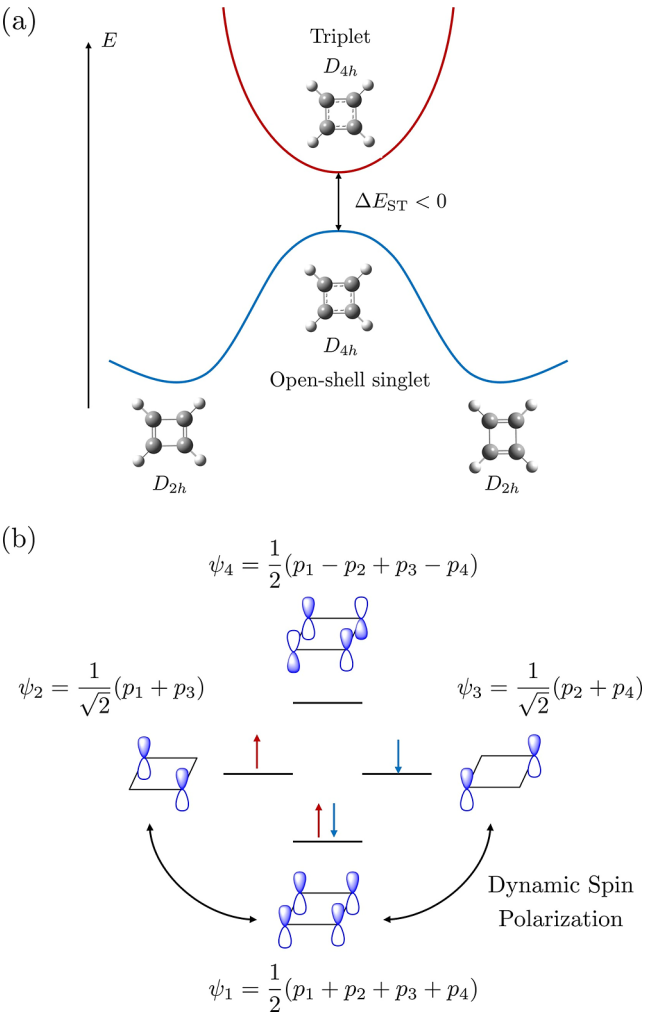

Figure 2. (a) Schematic representation of the ground-state and the first-excited-state PESs of CBD. For the square structure with a D_{4h} point group, the S−T gap ΔE_{ST} is negative. (b) Molecular orbital diagram of the square CBD. Electrons fill the orbitals in accordance with the configuration $|\psi_1^\alpha\psi_1^\beta\psi_2^\alpha\psi_3^\beta\rangle$.

symmetric double-well landscape and corresponds to the automerization involving the shifting of π bonds in CBD. The two equivalent equilibrium structures are rectangular because the structural distortion (D_{4h} to D_{2h}) results in a lowering of electronic energy (which is known as the second-order Jahn−Teller effect).[32] The singlet square CBD is higher in energy relative to the rectangular ones but still lies below the triplet excited state in the same geometry. The above-described two-orbital model fails to account for such an inverted S−T gap because it does not include any interaction between the unpaired electrons and the paired ones in the core orbitals. Figure 2b is a sketch of the molecular orbitals (ψ_1, ψ_2, ψ_3, ψ_4) of the square CBD obtained by taking linear combinations of the p_z orbitals (p_1, p_2, p_3, p_4) of the four carbon atoms. The doubly occupied orbital ψ_1 is the bonding π orbital and the degenerate orbitals ψ_2 and ψ_3 correspond to the singly occupied ψ_a and ψ_b in the two-orbital model. The electronic configuration depicted in Figure 2b can be denoted as $|\psi_1^\alpha\psi_1^\beta\psi_2^\alpha\psi_3^\beta\rangle$ and is a generalized representation of state |

Downloaded from pubs.acs.org/jctcce/article-pdf/21/17/8420/4126030/ct5c00942.pdf by PEKING UNIV user on 04 November 2026

https://doi.org/10.1021/acs.jctc.5c00942
J. Chem. Theory Comput. 2025, 21, 8420−8433

$|SB^1\rangle$ in Figure 1 that includes the bonding π electrons. Similarly, the other symmetry-broken state $|SB^2\rangle$ can be represented by $|\psi_1^\alpha\psi_1^\beta\psi_2^\beta\psi_3^\alpha\rangle$, and the linear combinations of $|\psi_1^\alpha\psi_1^\beta\psi_2^\alpha\psi_3^\beta\rangle$ and $|\psi_1^\alpha\psi_1^\beta\psi_2^\beta\psi_3^\alpha\rangle$ produce two eigenstates $|T_0\rangle$ and $|S_0^{OS}\rangle$.

The inclusion of the bonding and virtual orbitals is necessary here because the inverted S-T gap can only be explained by considering the configuration interaction (CI) between the open-shell singlet/triplet states and those configurations involving the excitation $\psi_1 \rightarrow \psi_4$. For the open-shell singlet state, the wave function of the two bonding electrons in ψ_1 is perturbed by the nonuniform distribution of the electronic spin in ψ_2 and ψ_3 and behaves as if the two bonding electrons are also "spin-polarized". This CI effect is referred to as *dynamic spin polarization*[33,55] (which distinguishes itself from the *static spin polarization* as the latter indicates real spin-density polarization in space) and significantly lowers the energies of singlet states for those diradicals with negative S−T gaps. On the contrary, the triplet states have polarized but uniformly distributed spins in ψ_2 and ψ_3, and are not substantially influenced by the CI effect. The idea of dynamic spin polarization provides an interpretation for the negative S−T gaps of diradicals because it correctly describes the electron correlation in a CI manner. Alternatively, a quantitative treatment of the electron correlation in diradicals may come from broken-symmetry DFT, as detailed in the following subsection.

2.2. Broken-Symmetry DFT. KS-DFT, as a single-determinantal theory, provides quantitative descriptions for qualitatively derived molecular orbitals (such as the diagram in Figure 2b) with relatively low computational expenses. To describe open-shell molecules like diradicals, one needs either a CI treatment or a broken-symmetry formulation of KS-DFT where a spin-unrestricted Slater determinant is used as a wave function ansatz. Here, we use the hydrogen molecule as a simple model to illustrate how broken-symmetry DFT functions for strongly correlated open-shell systems. In the following discussion, the two hydrogen atoms are labeled A and B, and their 1s orbitals are respectively denoted as ϕ_A and ϕ_B. The KS orbitals in RDFT are constructed from linear combinations of atomic orbitals. Hence the highest occupied (bonding) and the lowest unoccupied (antibonding) orbitals of H_2 are respectively constructed as

$$\phi_H = \frac{1}{\sqrt{2(1+S_{AB})}}(\phi_A + \phi_B)$$
$$\phi_L = \frac{1}{\sqrt{2(1-S_{AB})}}(\phi_A - \phi_B) \quad (4)$$

where $S_{AB} = \langle\phi_A|\phi_B\rangle$ is the overlap integral between ϕ_A and ϕ_B. The aufbau configuration of H_2 in RDFT is then $|\phi_H^\alpha\phi_H^\beta\rangle$. Recall that in states $|SB^1\rangle$ and $|SB^2\rangle$ from the two-orbital model, ψ_a and ψ_b are occupied by two electrons with different spins and have different spatial parts. This feature of ψ_a and ψ_b coincides with the spin-unrestricted KS orbitals in broken-symmetry DFT. In broken-symmetry DFT, the spatial parts of orbitals are different for electrons with different spins, that is, the set of KS orbitals $\{\phi\}$ in RDFT is reorganized into two different sets of spin−orbitals $\{\psi_a, \psi_b\}$, respectively occupied by spin-up and -down electrons. In the case of H_2, the closed-shell configuration $|\phi_H^\alpha\phi_H^\beta\rangle$ in RDFT turns into an open-shell configuration $|\psi_a^\alpha\psi_b^\beta\rangle$. One may construct the spin−orbitals by mixing the orbitals from RDFT, i.e.

$$\psi_a = c_H\phi_H + c_L\phi_L$$
$$\psi_b = c_H\phi_H - c_L\phi_L \quad (5)$$

where c_H and c_L are mixing coefficients satisfying $|c_H|^2 + |c_L|^2 = 1$. The outcome of replacing spin-restricted KS orbitals with spin-unrestricted orbitals is illustrated by Figure 3a. For the hydrogen molecule, RDFT assigns half spin-up and half spin-down electrons to each nucleus so that the wave function $|\phi_H^\alpha\phi_H^\beta\rangle$ retains the symmetry of the Hamiltonian and does not produce any local spin polarization in space. In contrast, broken-symmetry DFT assigns a spin-up(down) electron to nucleus A and a spin-down(up) electron to nucleus B, which breaks the spatial symmetry of spin-densities and gives rise to the two symmetry-broken states $|SB^1\rangle$ and $|SB^2\rangle$ described in the two-orbital model. Broken-symmetry DFT describes a specific correlation between the two unpaired electrons that is not available from RDFT: When a spin-up(down) electron is close to one of the nuclei, the electron with the opposite spin must be in the vicinity of the other.

Capturing such a specific electron correlation enables broken-symmetry DFT to provide a quantitatively correct description of the dissociating behavior of H_2. Figure 3b shows the binding energy of H_2 as a function of its bond length R produced by DFT calculations. One of the most commonly used DFA, the Perdew−Burke−Ernzerhof (PBE) functional,[56] is used to evaluate the XC energy. As is shown in Figure 3b, RDFT serves as a good approximation to the exact energy near the equilibrium bond length since the molecule stays closed-shell and has weakly correlated electrons in that region. When the molecule is stretched beyond the Coulson−Fischer (CF) point[57] and enters the regime of strong electron correlation, RDFT severely overestimates its energy. Conversely, broken-symmetry DFT yields results in good agreement with the exact theory throughout the entire range of bond lengths. The broken-symmetry solution $|SB^1\rangle$ (or $|SB^2\rangle$) captures the electron correlation embodied in the true open-shell singlet state $|S_0^{OS}\rangle$ of H_2. The generic relation between the energies of these two states reads

$$E_S = \frac{E_{SB} + H_{12}}{1 + S_{12}} \quad (6)$$

where $E_{SB} = \langle SB^1|H|SB^1\rangle = \langle SB^2|H|SB^2\rangle$ and $H_{12} = \langle SB^1|H|SB^2\rangle$ are the diagonal and off-diagonal matrix elements of the Hamiltonian, respectively, and E_S is the energy of the open-shell singlet state $|S_0^{OS}\rangle$. For H_2 with very large bond lengths ($R \rightarrow \infty$), the two-orbital model represents an essentially exact description and dictates that

$$S_{12} = -S_{ab}^2 \rightarrow 0, \qquad H_{12} = -h_{ab}S_{ab} - K_{ab} \rightarrow 0 \quad (7)$$

We define a spin-unrestricted KS wave function fulfilling eq 7 as an *ideal* broken-symmetry state since it has the same energy as the open-shell singlet state.

One criterion for determining whether a broken-symmetry state is ideal or not is the local net spin populations of the radical centers, which is related to the diradical character y defined by Nakano and Champagne.[58] The diradical character measures the instability of chemical bonds in open-shell

Downloaded from pubs.acs.org/jctce/article-pdf/21/17/8420/4126030/ct5c00942.pdf by PEKING UNIV user on 04 November 2026

https://doi.org/10.1021/acs.jctc.5c00942
J. Chem. Theory Comput. 2025, 21, 8420−8433

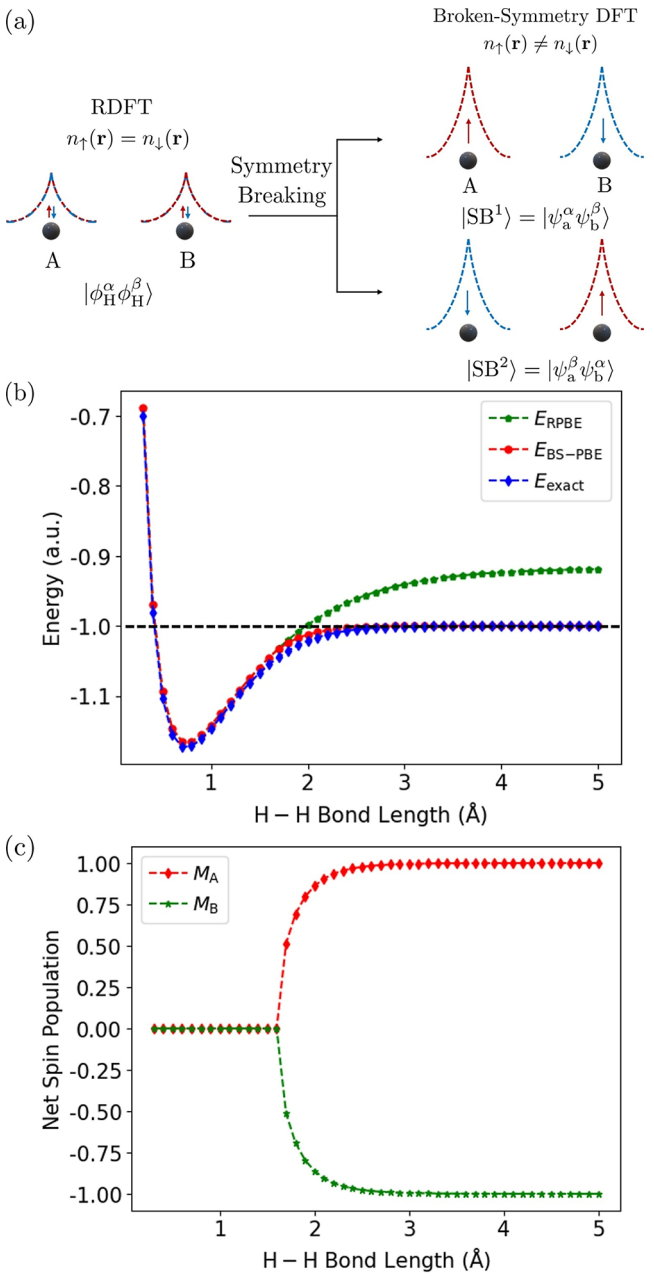

Figure 3. (a) Schematic representation of spin-densities $n_\uparrow(r)$ and $n_\downarrow(r)$ of a stretched hydrogen molecule, obtained from RDFT and broken-symmetry DFT calculations. The spin-up and spin-down electron densities are labeled in red and blue, respectively. (b) Dissociation curves of H_2 calculated with RDFT (green) and broken-symmetry DFT (red) using PBE as the DFA. The dashed black line marks the dissociation limit. The exact curve marked in blue is calculated at the CCSD/cc-pVQZ level of theory. (c) Net spin populations ($M = N_\uparrow - N_\downarrow$) of atoms A and B in a hydrogen atom as functions of the bond length, extracted from broken-symmetry DFT calculations using PBE as the DFA.

systems: $y = 0$ suggests the molecule is closed-shell while $y = 1$ indicates a pure diradical. Molecules with intermediate values ($0 < y < 1$) are known as *diradicaloids*. To clarify the relationship between the diradical character and local spin populations, we reexamine the dissociation problem of H_2. Note that eq 5 can be rewritten in terms of the atomic orbitals ϕ_A and ϕ_B

$$\psi_a = c_1\phi_A + c_2\phi_B$$
$$\psi_b = c_2\phi_A + c_1\phi_B \tag{8}$$

where

$$c_1 = \frac{c_H}{\sqrt{2(1+S_{AB})}} + \frac{c_L}{\sqrt{2(1-S_{AB})}},$$
$$c_2 = \frac{c_H}{\sqrt{2(1+S_{AB})}} - \frac{c_L}{\sqrt{2(1-S_{AB})}} \tag{9}$$

It is evident that the diradical character is determined by c_1 and c_2: if $c_1 = c_2$, eq 8 yields $\psi_a = \psi_b = \phi_H$ and indicates a closed-shell system ($y = 0$). If $c_1 = 1$ and $c_2 = 0$, the spin-unrestricted orbitals become identical to the atomic orbitals and are completely localized on atoms A and B ($\psi_a = \phi_A$, $\psi_b = \phi_B$), corresponding to a pure diradical with $y = 1$. One may also notice that the net spin populations of radical centers (here the two hydrogen atoms A and B) are also related to c_1 and c_2 since eq 8 is written in terms of atomic orbitals. For state $|SB^1\rangle = |\psi_a^\alpha \psi_b^\beta\rangle$, the net spin populations of atoms A and B are

$$M_A = |c_1|^2 - |c_2|^2, \qquad M_B = |c_2|^2 - |c_1|^2 \tag{10}$$

respectively. The outcome of eq 10 is consistent with the discussion on the diradical character because $c_1 = c_2$ generates a spin-neutral closed-shell regime ($M_A = M_B = 0$) whereas $c_1 = 1$, $c_2 = 0$ leads to a full spin localization on different radical centers ($M_A = 1$, $M_B = -1$). This connection between the diradical character and the net spin populations of radical centers is verified by Figure 3c, which depicts the net spin populations of atoms A and B as functions of the bond length R, extracted from broken-symmetry DFT calculations. As shown in Figure 3c, the polarization of spin populations appears at the CF point and gradually strengthens as the bond length increases. In the dissociation limit, the spin populations exhibit the correct asymptotic behavior of having a spin-up electron on atom A and a spin-down electron on atom B ($M_A \to 1$, $M_B \to -1$), in accordance with the fact that the dissociated H_2 is a pure diradical. The solution given by broken-symmetry DFT, in this case, introduces only essential symmetry breaking and thus represents an ideal broken-symmetry state for H_2. The corresponding spin populations on the hydrogen atoms in this limit, $M_A = +1$ and $M_B = -1$ (or vice versa), are defined as the *ideal spin populations* for the dissociated hydrogen molecule. The concept of ideal spin populations serves as a crucial quantity in SR-PDFT, which will be introduced later in Section 2.3.

Based on the above analysis, we conclude that broken-symmetry DFT accurately accounts for the static correlation experienced by H_2. The broken-symmetry solution does not suffer from artificial symmetry breaking and thus produces correct energetics. For other diradicals with more than two electrons, the off-diagonal matrix element H_{12} and the overlap integral S_{12} cannot simply be evaluated in terms of the two frontier orbitals ψ_a and ψ_b. Broken-symmetry DFT often leads to artificial symmetry breaking for these systems because it typically polarizes the spin of the electrons in the core orbitals. As a result, the broken-symmetry solution does not necessarily reflect the correct electron correlation embodied in those complex systems. A quantitatively correct description of these complex diradicals requires broken-symmetry DFT to break only certain symmetries that are considered essential. It was suggested by Lee et al. that one can distinguish between

Downloaded from pubs.acs.org/jctce/article-pdf/21/17/8420/4126030/ct5c00942.pdf by PEKING UNIV user on 04 November 2026

https://doi.org/10.1021/acs.jctc.5c00942
J. Chem. Theory Comput. 2025, 21, 8420−8433

essential and artificial symmetry breaking in the broken-symmetry solution by performing the regularized orbital-optimized MP2 (κ-OOMP2) calculations.[49] Since the present work focuses on DFT, we endeavor to avoid the complexity of performing post-Hartree−Fock calculations. Alternatively, we propose the following conjecture to relate the idea of essential symmetry breaking to the diradical character of molecules: The symmetry breaking is essential if and only if the two strictly degenerate frontier orbitals of a pure diradical ($y = 1$) are separately occupied by two electrons whose spins are fully polarized, as observed in the broken-symmetry solution for the dissociated hydrogen molecule. For molecules with $0 < y < 1$, essential symmetry breaking distributes two electrons with partially polarized spins on their frontier orbitals. The hydrogen molecule is a pure diradical in its dissociation limit, so the symmetry breaking that fully polarizes the spins of its two electrons is essential. Contrarily, the broken-symmetry DFT solution for the square CBD suffers from the problem of artificial symmetry breaking and thus is not an ideal broken-symmetry state. Considering the high structural symmetry of the square CBD, we conjecture that it is also a pure diradical since it has two strictly degenerate and spatially separated frontier orbitals belonging to the E_g irreducible representation of the D_{4h} point group. Then, the symmetry breaking is essential when the frontier orbitals of CBD are separately occupied by two electrons with opposite spins. Such a constraint is not satisfied by broken-symmetry DFT. Artificial symmetry breaking leads to an overestimation of the degree of spin polarization in the radical centers (in this case, the four CH groups), so broken-symmetry DFT predicts the diradical character of the square CBD to be greater than unity. The overestimation of local spin polarization yields nonzero H_{12} and S_{12} in eq 6. Consequently, the broken-symmetry state does not have the same energy as the open-shell singlet state anymore.

2.3. SR-PDFT. We first briefly summarize the formalism of PDFT, for which comprehensive reviews are available,[52,59] and then discuss the implementation of the SR procedure and its correction to the nonadditive XC energy.

The first step is to partition the molecule into N_f noninteracting fragments by dividing the external nuclear potential $v(\boldsymbol{r})$ as

$$v(\boldsymbol{r}) = \sum_i^{N_f} v_i(\boldsymbol{r}) \tag{11}$$

where $v_i(\boldsymbol{r})$ is the external potential of the ith fragment. Self-consistent KS-DFT calculations are performed for fragments to obtain their ground-ensemble energies E_i and corresponding densities $n_i(\boldsymbol{r})$. This is done by minimizing the sum of fragment energies $E_f \equiv \sum_i E_i$ subject to the constraint

$$n_f(\boldsymbol{r}) \equiv \sum_i n_i(\boldsymbol{r}) = n_m(\boldsymbol{r}) \tag{12}$$

where $n_m(\boldsymbol{r})$ is the molecular ground-state density corresponding to $v(\boldsymbol{r})$. The fragment energies $E_i[\{n_i\}]$ are functionals of the set of fragment densities, and can be decomposed in terms of the usual Kohn−Sham quantities as $E_i[n_i] = T_s[n_i] + E_{ext}[n_i] + E_H[n_i] + E_{XC}[n_i]$, where $E_{ext}[n_i]$ is the "external" energy of $N_i = \int d\boldsymbol{r} n_i(\boldsymbol{r})$ electrons in the potential $v_i(\boldsymbol{r})$. Since the fragments in PDFT are noninteracting, an extra term E_p is included in the total energy to account for the interactions between fragments. The total energy then reads

$$E[\{n_i\}] = E_f[\{n_i\}] + E_p[\{n_i\}] \tag{13}$$

where E_p (the "partition energy"), can also be decomposed in terms of KS quantities

$$E_p[\{n_i\}] = T_s^{nad}[\{n_i\}] + E_{ext}^{nad}[\{n_i\}] + E_H^{nad}[\{n_i\}] + E_{XC}^{nad}[\{n_i\}] \tag{14}$$

In the broken-symmetry formulation, the nonadditive energy $W^{nad}[\{n_i\}]$ ($W = T_s, E_{ext}, E_H$, or E_{XC}) should be generalized to a spin-resolved form: $W^{nad}[\{n_{i\uparrow}, n_{i\downarrow}\}] = W[n_{f\uparrow}, n_{f\downarrow}] - \sum_i W[n_{i\uparrow}, n_{i\downarrow}]$.

To allow the fragments to possess a fractional number of electrons or spins, they are treated either as ensembles (ENS)[60] or with the fractional orbital occupation (FOO)[61] approach. The ENS treatment expresses a fragment property as a weighted sum of multiple contributing states. For instance, the XC energy of fragment i is given by

$$E_{XC,i}[n_{i\uparrow}, n_{i\downarrow}] = \sum_j^{N_{ENS}} f_{ij} E_{XC,ij}^{ENS}[n_{ij\uparrow}, n_{ij\downarrow}] \tag{15}$$

where the index j runs over N_{ENS} ensemble components, and f_{ij} is the contribution weight of the j-th ensemble state to fragment i. Note that the (averaged) spin-density $n_{i\uparrow(\downarrow)}$ can integrate to noninteger values, while the ensemble components $n_{ij\uparrow(\downarrow)}$ correspond to pure states that always have integer numbers of spins. On the other hand, the FOO approach describes fragments with noninteger electron and spin numbers by directly feeding spin-densities (which integrate to noninteger values) into the DFA, leading to a single-term expression for the XC energy $E_{XC,i}^{FOO}[n_{i\uparrow}, n_{i\downarrow}]$. In principle, if the exact XC functional were available, the FOO and ensemble representations would lead to the same results.[60] However, those two representations make a significant difference in approximate PDFT calculations.[62,63]

PDFT is well suited for applications to disjoint diradicals that can be partitioned into fragments containing a radical center. The net spin population M_i of fragment i is simply

$$M_i = \int d\boldsymbol{r}[n_{i\uparrow}(\boldsymbol{r}) - n_{i\downarrow}(\boldsymbol{r})] \tag{16}$$

Equation 16 provides a convenient way of tuning the degree of spin polarization in the molecule. Given the ideal net spin populations of all radical centers $\{M_i^{id}\}$ free from artificial symmetry breaking, the corresponding spin-densities $\{n_{i\sigma}^{SR}\}$ can be obtained from PDFT via the SR procedure that enforces $M_i = M_i^{id}$. Based on these quantities, we introduce an SR-based correction that can remove both intrinsic errors of DFAs and the effects of artificial symmetry breaking, by incorporating a portion of FOO-represented fragment XC energies into the original expression for the nonadditive XC energy in its ENS representation

$$E_{XC}^{nad,SR} = E_{XC}^{nad,ENS}[\{n_{i\sigma}^{DFA}\}] + g\kappa\{E_{XC}[\{n_{i\sigma}^{DFA}\}] - \sum_i^{N_f} E_{XC,i}^{FOO}[\{n_{i\sigma}^{SR}\}]\} \tag{17}$$

where $n_{i\sigma}^{DFA}$ is the unregularized spin-density from the DFA with σ specifying the spin state, $n_{i\sigma}^{SR}$ is the regularized spin-density obtained after the SR procedure,

Downloaded from pubs.acs.org/jctce/article-pdf/21/17/8420/4126803O/ct5c00942.pdf by PEKING UNIV user on 04 November 2026

https://doi.org/10.1021/acs.jctc.5c00942
J. Chem. Theory Comput. 2025, 21, 8420−8433

$E_{XC}^{nad,ENS}[\{n_{i\sigma}^{DFA}\}] = E_{XC}[\{n_{i\sigma}^{DFA}\}] - \sum_{i}^{N_f}\sum_{j}^{N_{ENS}} f_{ij} E_{XC,ij}^{ENS}[\{n_{i\sigma}^{DFA}\}]$ is the ENS-expressed nonadditive XC energy obtained from broken-symmetry calculations using a given DFA, and the second term on the right-hand side quantifies the extent to which the XC energy is underestimated as a result of artificial symmetry breaking, with g and κ acting as scaling factors. The total XC energy $E_{XC}[\{n_{i\sigma}^{DFA}\}]$ includes the contributions from both essential and artificial symmetry breaking, while the FOO-represented XC energies of fragments ($E_{XC,i}^{FOO}[\{n_{i\sigma}^{SR}\}]$) capture only essential symmetry breaking within the fragments, since they are evaluated from regularized spin-densities. Thus, the artificial symmetry breaking effects are isolated in the difference between the two terms enclosed in the large curly braces of eq 17. It should be noted that this difference also contains the interfragment contribution from essential symmetry breaking to the XC energy, which must be preserved in any approximation designed to eliminate only the artificial symmetry-breaking error. To achieve this, we introduce a scaling factor κ that quantifies the portion of the difference attributable solely to artificial symmetry breaking

$$\kappa(|M_i^{DFA} - M_i^{id}|) = -\frac{1}{N_f}\sum_{i=1}^{N_f}\frac{|M_i^{DFA} - M_i^{id}|}{2N_i} \tag{18}$$

Equation 18 measures the difference in local net spin populations between an ideal broken-symmetry state (includes only essential symmetry breaking) and a broken-symmetry state from a given DFA (includes both essential and artificial symmetry breaking) $|M_i^{DFA} - M_i^{id}|$, with N_i in the denominator representing the total number of electrons in fragment i.

The second prefactor g is introduced to account for the DFA-dependent error contributions to the XC energy. Different DFAs not only yield electron densities with different degrees of spin polarization but also a have direct impact on the XC energy itself, e.g, how fast the XC energy varies as the spin polarization develops. Even if the same spin-densities are used, the XC energy will depend on the choice of DFA. Here, g is designed to be a function of the following quantity

$$s_{DFA} = \frac{1}{N_f}\sum_{i=1}^{N_f}\left|\left(\frac{\partial E_{XC}^{DFA}}{\partial M_i}\bigg|_{M_i=M_i^{id}}\right)\right| \tag{19}$$

which is an intrinsic property of DFAs that quantifies the sensitivity to change of E_{XC} (from a given DFA) with respect to the local spin polarization in molecules. For simplicity, the derivative is taken when the spin population equals that in an ideal broken-symmetry state. The function g has the form

$$g(s_{DFA}) = \pm\left(\frac{s_{DFA}}{s_{PBE}}\right)^2 \tag{20}$$

in which the positive (negative) sign applies when E_{XC} is concave (convex) with respect to M_i. Here, PBE is used as a reference functional, so $g(s_{PBE}) = 1$. Substituting E_{XC}^{nad} in eq 14 with $E_{XC}^{nad,SR}$ leads to a correction to the partition energy, and thus to the total energy, which removes the effects of artificial symmetry-breaking while retaining those of essential symmetry breaking. This ensures the SR-PDFT solution aligns with the ideal broken-symmetry state.

3. COMPUTATIONAL METHODS

Broken-symmetry DFT calculations for molecules were performed with the PySCF[64−66] quantum chemistry package. Fragment calculations were done using a PDFT implementation in PySCF. Dunning's correlation consistent basis set of quadruple-ζ quality (cc-pVQZ)[67] was used for all the molecules and fragments. Molecular geometries along the minimum energy paths of the CBD automerization reactions were generated using the intrinsic reaction coordinate (IRC) module of Gaussian 16 (C.02)[68] software package. The details of molecular coordinates and ensemble set-ups can be found in the Supporting Information. The partition potential

$$v_p(\mathbf{r}) = \frac{\delta E_p[\{n_i\}]}{\delta n_i(\mathbf{r})} \tag{21}$$

is updated iteratively by adding the difference between the molecular density and the sum of fragment densities

$$v_p^{(k+1)} = v_p^{(k)} + \lambda(n_f - n_M) \tag{22}$$

where $v_p^{(k)}$ represents the partition potential in the k-th iteration and λ is the step size of updating v_p. The convergence is achieved when $n_f(\mathbf{r}) = n_M(\mathbf{r})$. The SR correction was introduced in a postconvergence manner, i.e., the quantities κ, g, and the nonadditive XC energies in eq 17 are evaluated with converged fragment spin-densities. The code used for all PDFT calculations is available on GitHub at https://github.com/yishi62751/SR-PDFT.git.

4. RESULTS AND DISCUSSION

In this section, we first show the minimum energy path (MEP) of the automerization of CBD obtained from broken-symmetry DFT calculations with six commonly used DFAs. We then find the ideal net spin populations of radical centers in CBD that correspond to essential symmetry breaking and, finally, apply the SR procedure of Section 2.3 to demonstrate improvements over broken-symmetry DFT.

4.1. Broken-Symmetry DFT. Broken-symmetry DFT eliminates static correlation errors of DFAs by breaking spin symmetries. Unlike the case of H_2 in Section 2.2, which exemplifies essential symmetry breaking, the automerization of CBD suffers from artificial symmetry breaking. To benchmark the performance of standard DFAs, we selected six representative functionals across three rungs of Perdew's Jacob's ladder[69] and applied broken-symmetry DFT to investigate the PES of CBD automerization. We label the four CH groups in CBD clockwise as 1, 2, 3, and 4 (consistent with the way CBD is partitioned in PDFT). The automerization involves alternating bond length changes: As C_1-C_2/C_3-C_4 bonds lengthen, C_2-C_3/C_4-C_1 bonds shorten, and vice versa. The evolution of CBD's total energy along the MEP is shown by plotting it against the C_1-C_2 bond length in Figure 4a. Six common DFAs were used in broken-symmetry DFT to calculate the energies of a series of structures on an MEP generated by broken-symmetry DFT calculations at the PBE/cc-pVQZ level of theory. The end points of the MEP correspond to the two equivalent equilibrium structures of CBD, which we set as the zero point of energy for all DFAs, and the midpoint represents the transition state, so the vertical

Downloaded from pubs.acs.org/jctce/article-pdf/21/17/8420/4126030/ct5c00942.pdf by PEKING UNIV user on 04 November 2026

https://doi.org/10.1021/acs.jctc.5c00942
J. Chem. Theory Comput. 2025, 21, 8420−8433

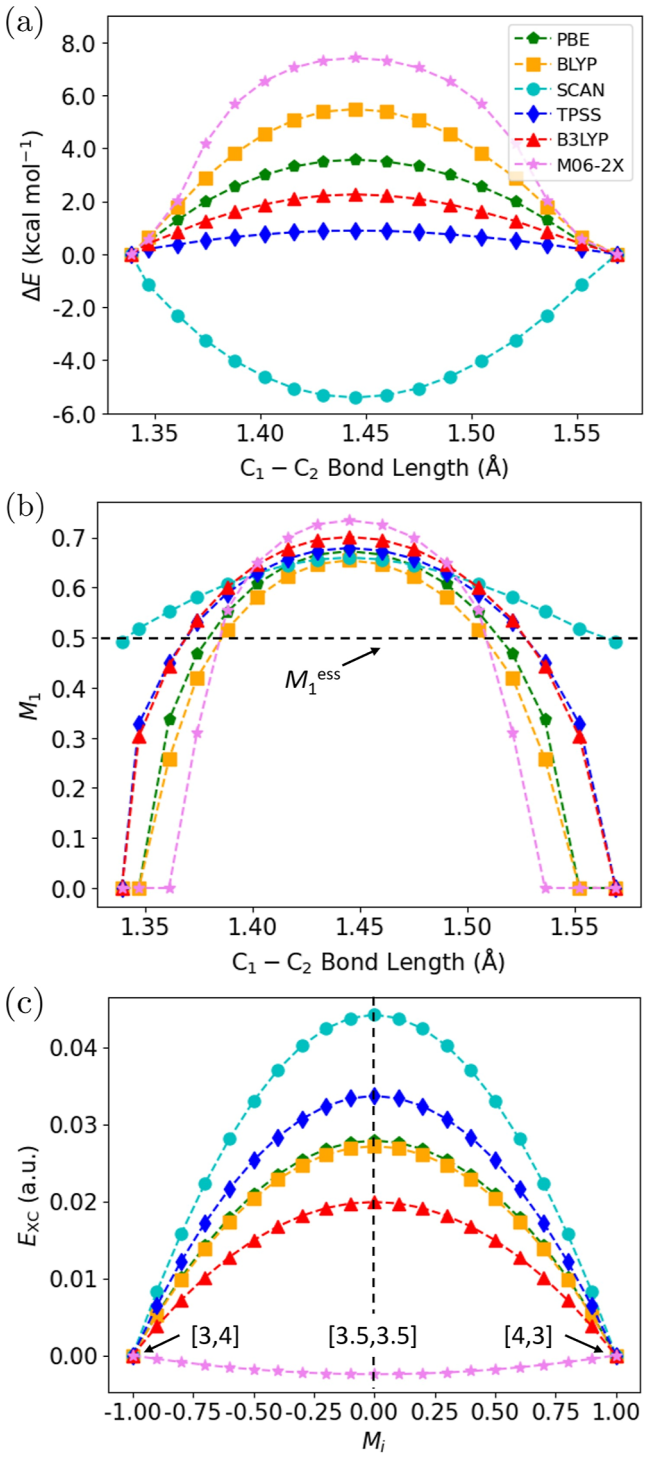

Figure 4. (a) Minimum energy paths of CBD automerization, calculated with broken-symmetry DFT using six common DFAs. The paths are generated following the direction of stretching the bond C_1−C_2. (b) Net spin populations of fragment **1** as a function of the C_1−C_2 bond length, extracted from broken-symmetry DFT. The proper supremum of M_1 given by essential symmetry breaking is marked by the dashed black line. (c) Dependence of the XC energy of the square CBD on the local net spin population of fragments. Brackets $[N_\uparrow, N_\downarrow]$ indicate the number of spin-up and -down electrons for a certain value of M_i.

axis ΔE refers to the energy difference between a given structure and the equilibrium geometry of CBD. Table 1 lists

Table 1. Automerization Barrier Height E_b of CBD Evaluated With Broken-Symmetry DFT Using Common DFAs

method	E_b (kcal mol^{-1})[a]
PBE	3.6
BLYP	5.5
SCAN	−5.4
TPSS	0.9
B3LYP	2.3
M06−2X	7.4
reference[b]	8.6−10.9

[a]The reported barrier heights are purely electronic and do not include zero-point vibrational energy corrections. [b]Reference values were obtained from previous state-of-the-art multireference quantum chemical calculations.[37,38,45,46]

the height of the automerization barrier extracted from the MEPs shown in Figure 4a, along with the reference values obtained from multiconfigurational wave function methods. As we can see from Figure 4a and Table 1, all six DFAs underestimate the barrier height of the automerization. The generalized gradient approximations (GGAs), PBE and BLYP, predict positive but underestimated barrier heights compared to reference values. Meta-GGAs perform even worse: TPSS produces a substantially small barrier height, and SCAN erroneously places the transition state below the equilibrium structure. Hybrid functionals exhibit fundamentally distinct behaviors due to the incorporation of exact exchange and their diverse parametrization schemes. The two most widely used hybrid functionals show dramatic differences: B3LYP yields a barrier lower than GGAs, while M06−2X provides an unexpectedly accurate barrier height, nearly matching the lower bound of reference values.

To understand why broken-symmetry DFT underestimates the height of the automerization barrier, consider the local spin polarizations of CBD. Again, we label the four CH fragments clockwise as 1, 2, 3, and 4. According to Figure 2b, the two frontier orbitals ψ_2 and ψ_3 of the square CBD are distributed on nonadjacent fragments. For square CBD to be a pure diradical, ψ_2 and ψ_3 should be singly occupied by two unpaired electrons with opposite spins. In an ideal broken-symmetry state, fragments 1 and 3 share a spin-up electron, and fragments 2 and 4 share a spin-down electron, or vice versa. The corresponding ideal net spin populations of the four CH fragments should be $M_1 = 0.5$, $M_2 = -0.5$, $M_3 = 0.5$, and $M_4 = -0.5$ (or $M_1 = -0.5$, $M_2 = 0.5$, $M_3 = -0.5$, and $M_4 = 0.5$). Broken-symmetry DFT overestimates the degree of local spin polarization in the square transition state of CBD, as can be seen from Figure 4b, which plots the net spin population of fragment 1 along the MEP. As in the case of H_2, the spin-densities/populations stay neutral near the equilibrium structure and become polarized when the C_1−C_2 bond is stretched beyond the CF point, although the precise position of this point varies among DFAs. The spin polarization exhibits a gradual enhancement following the CF point and reaches its maximum value at the square transition state. We claim that in an ideal broken-symmetry state, the behavior of the spin-density should obey the constraint given by essential symmetry breaking: The net spin populations of fragments should be approaching a supremum $M_i^{ess} = \pm 0.5$ as the degree of spin polarization increases. As can be seen in Figure 4b, none of the six DFAs follow this behavior. Spin polarization occurs when

Downloaded from pubs.acs.org/jctce/article-pdf/21/17/8420/4126030/ct5c00942.pdf by PEKING UNIV user on 04 November 2026

https://doi.org/10.1021/acs.jctc.5c00942
J. Chem. Theory Comput. 2025, 21, 8420−8433

Table 2. SR Correction for the Automerization Transition State Given by Common DFAs

DFA	E_{XC} (a.u.)	ΔE_{XC}[a] (a.u.)	$g(s_{DFA})$	κ	SR correction[b] (kcal mol^{-1})
PBE	−22.8909	−0.6776	1.0000	0.0124	5.2
BLYP	−23.0508	−0.6174	0.9504	0.0111	4.1
SCAN	−23.0224	−0.7622	2.5588	0.0114	14.0
TPSS	−23.1523	−0.6860	1.4512	0.0129	8.0
B3LYP	−18.7030	−0.5201	0.5106	0.0144	2.4
M06−2X	−11.1408	−0.2794	−0.0077	0.0168	0.0

[a]The quantity ΔE_{XC} is the difference enclosed by the large curly braces on the right-hand side of eq 17: $\Delta E_{XC} = E_{XC}[\{n_{i\sigma}^{DFA}\}] - \sum_{i}^{N_f} E_{XC,i}^{FOO}[\{n_{i\sigma}^{SR}\}]$.

[b]The SR correction refers to the correction to the nonadditive XC energy, i.e., $g\kappa\Delta E_{XC}$.

the bond C_1-C_2 is stretched 0.01−0.02 Å away from the equilibrium structure, and exceeds the supremum imposed by essential symmetry breaking well before the molecule is in close structural proximity to the transition state. All tested DFAs predict similar spin polarization magnitudes for the transition state, with results confined to a limited range between 0.65 (BLYP) and 0.73 (M06−2X). Notably, the SCAN functional even predicts a spin-polarized equilibrium structure leading to a negative barrier height.

The overestimation of local spin polarization in broken-symmetry DFT has a direct impact on the XC energy. Figure 4c demonstrates the dependence of the XC energy on the net spin population of the i-th CH fragment M_i. Figure 4c is done with PDFT by calculating the XC energy of CBD at the transition state geometry when varying the net spin populations of the fragments. Brackets $[N_\uparrow, N_\downarrow]$ represent the number of spin-up and spin-down electrons in fragment i. The end points stand for the case where one electron is fully spin-polarized, which are set as the energy zero points for all DFAs, and the midpoint stands for the spin-unpolarized case. As illustrated in Figure 4c, the XC energy calculated with most DFAs is a concave function of M_i (except for M06−2X). In other words, the XC energy from typical DFAs decreases with increasing spin polarization. Therefore, the consequence of overestimating local spin polarization in broken-symmetry DFT is an underestimation of the XC energy. This is undoubtedly the main reason why DFAs underestimate the energy of the transition state. To explain why different DFAs result in different barrier heights when the degrees of local spin polarization are similar (e.g., BLYP and SCAN both lead to $M_i \sim \pm 0.65$, but the resulting barrier heights are dramatically different), we note that the derivative of the XC energy with respect to the net spin population, measured by s_{DFA} as defined in eq 19, varies with the choice of DFA. According to Figure 4c, $s_{BLYP} < s_{SCAN}$, so SCAN is more sensitive to the change in local net spin populations. Given that $M_i^{BLYP} \approx M_i^{SCAN}$ for the transition state, SCAN lowers the XC energy much more than BLYP. This significant energy reduction causes SCAN to incorrectly place the transition state below the equilibrium structure in energy. Meta-GGAs are more sensitive to the change in the degree of local spin polarization than GGAs, and that is why the use of meta-GGAs produces lower reaction barriers. The hybrid functionals are fundamentally different because of the incorporation of exact exchange. As shown in Table 2, while semilocal DFAs (GGAs and meta-GGAs) produce numerically similar XC energy magnitudes, hybrid functionals generate markedly different results. B3LYP and M06−2X increase the XC energy to about −18 and −11 au, respectively. Even more crucially, M06−2X does not follow the typical behavior of DFAs. The XC energy produced by M06−2X is a convex function of M_i, so the spin polarization increases the XC energy instead. This feature of M06−2X explains why it yields a higher barrier compared to other DFAs. In the following subsection, we demonstrate the implementation of the SR correction within the PDFT framework and systematically assess the performance of DFAs under this correction.

4.2. SR-PDFT. In Section 2.3, we introduced the basic idea of SR-PDFT. We now detail the implementation of the SR correction and demonstrate how it improves upon broken-symmetry DFT.

Using PDFT, we divide CBD into four CH fragments, each representing a radical center in the transition state. To compute the SR-corrected nonadditive XC energy in eq 17, we need: (i) the unregularized spin-densities of fragments $\{n_{i\sigma}^{DFA}\}$ that are obtained from broken-symmetry DFT calculations with certain DFAs, and (ii) the regularized fragment spin-densities $\{n_{i\sigma}^{SR}\}$ generated by SR-PDFT. Atom-condensed spin populations are accessible from broken-symmetry DFT, so the fragment spin populations $\{M_i^{DFA}\}$ can be readily obtained by summing up the broken-symmetry DFT spin populations of carbon and hydrogen atoms in each fragment. We then adjust the ensemble weights to ensure that the numbers of spin-up and spin-down electrons in each fragment match those given by M_i^{DFA}'s (see Section S1 of the Supporting Information). This guarantees that PDFT recovers the broken-symmetry DFT results, as the sum of the fragment spin-densities equals the total molecular spin-density obtained from broken-symmetry DFT. The real difficulty lies in finding the net spin populations of fragments in an ideal broken-symmetry state, $\{M_i^{id}\}$, from which we can further find the regularized spin-densities of fragments $\{n_{i\sigma}^{SR}\}$. Since the spin symmetry breaking in the case of H_2 is considered completely essential, we claim that the ideal fragment spin populations M_i^{id}'s of CBD should exhibit a pattern similar to M_i^{DFA}'s of H_2. Specifically, the molecule should stay spin-unpolarized from the equilibrium geometry to the CF point along the MEP, and near the transition state geometry, the essential symmetry breaking should yield fragment net spin populations of approximately ±0.5. However, the ideal fragment spin populations, $\{M_i^{id}\}$, remain undetermined for those geometries between the CF point and the transition state. To avoid the complication of distinguishing essential and artificial symmetry breaking for each structure (typically requiring κ-OOMP2[49] calculations), we introduce a model function describing the complete essential symmetry breaking process, following the spin polarization pattern observed in broken-symmetry DFT

https://doi.org/10.1021/acs.jctc.5c00942
J. Chem. Theory Comput. 2025, 21, 8420−8433

Downloaded from pubs.acs.org/jctce/article-pdf/21/17/8420/4126030/ct5c00942.pdf by PEKING UNIV user on 04 November 2026

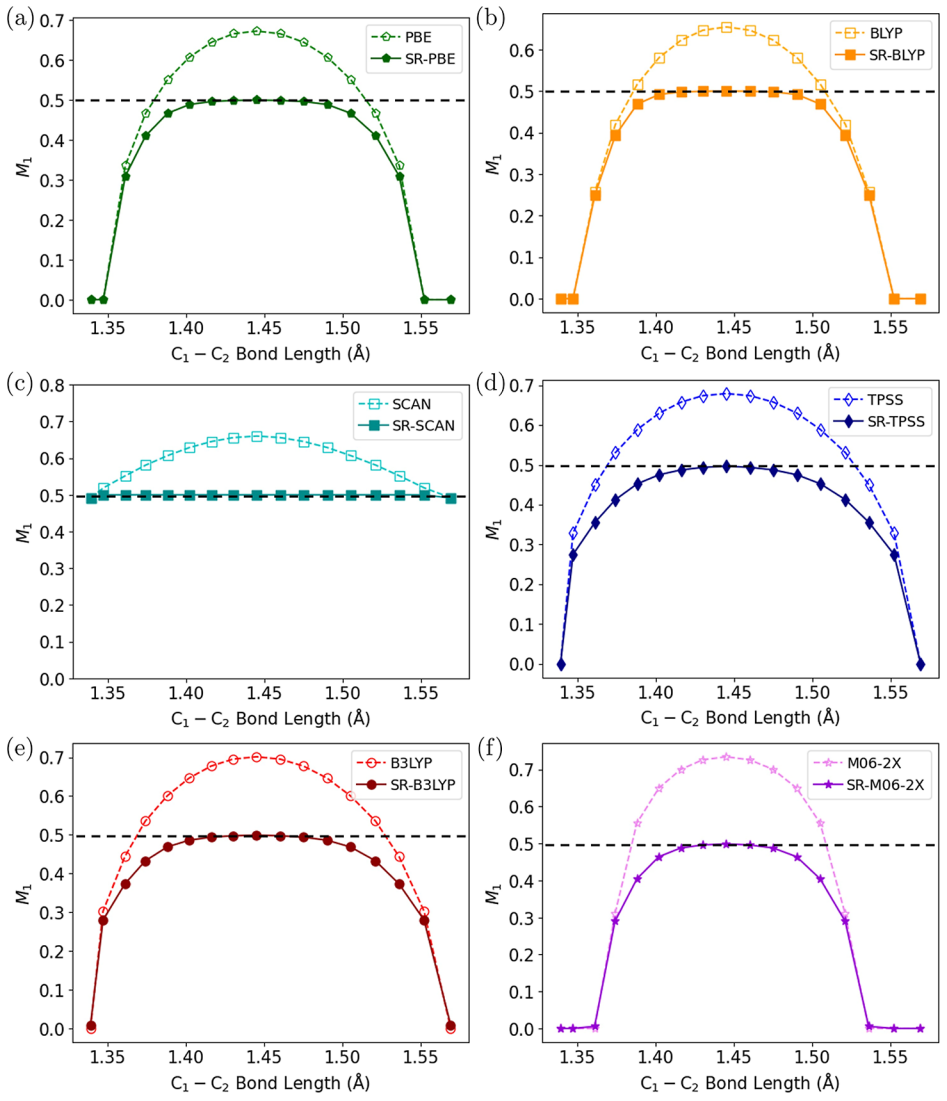

Figure 5. Net spin populations of fragment **1** as a function of the C_1−C_2 bond length, extracted from broken-symmetry DFT calculations done with (a) PBE, (b) BLYP, (c) SCAN, (d) TPSS, (e) B3LYP, and (f) M06−2X functionals, along with the ideal net spin populations of fragment 1 generated from the SR procedure. The ideal spin populations are used in SR-PDFT calculations. The proper supremum of M_1 corresponding to essential symmetry breaking of the transition state is marked by the dashed black line.

for H_2. This function should satisfy two conditions: (i) an abrupt transition in spin populations near the CF point, and (ii) a gradual approach to the limiting values ($M_i^{\mathrm{ess}} = \pm 0.5$) at the transition-state structure. The proposed functional form is

$$M_i^{\mathrm{id}}(R) = \begin{cases} \dfrac{M_i^{\mathrm{ess}}}{1 + e^{-k_1(R-R_t)}}, & \text{if } R \le R_t \\ \dfrac{M_i^{\mathrm{ess}}}{1 + e^{-k_2(R-R_t)}}, & \text{if } R > R_t \end{cases} \tag{23}$$

where R_t is the transition point where spin polarization occurs (generally deviates slightly from the CF point to produce a spin polarization pattern resembling that of H_2), and k_1 and k_2 are parameters controlling the rate of change in the net spin populations near R_t. In most cases, $k_1 \gg k_2$, as the spin polarization emerges sharply when R approaches R_t from the left and strengthens progressively for $R > R_t$. Parametrization is needed for each DFA, and all parameters are provided in Section S2 of the Supporting Information. Note that while the spin populations for the equilibrium structure and transition state are rigorously determined by the condition enforced by essential symmetry breaking, intermediate points only represent approximations to the ideal broken-symmetry state. For molecules with diradical characters smaller than one, a robust method for determining ideal spin populations remains a desirable goal for future work.

Figure 5 depicts the ideal fragment net spin populations generated by the model function. The original fragment spin populations extracted from broken-symmetry DFT results are also plotted for comparison. As we can see in Figure 5, the ideal spin populations remain zero or negligible (except for SCAN) near the equilibrium structure, and gradually increase until reaching M_i^{ess} at the transition state. The difference between the two sets of spin populations, $|M_i^{\mathrm{DFA}} - M_i^{\mathrm{id}}|$, is negligible at the equilibrium geometry of CBD and increases steadily along the MEP toward the transition state. Consequently, the quantity κ defined in eq 18 yields the largest correction for the transition state and does not significantly influence the energy of the equilibrium structure.

Downloaded from pubs.acs.org/jctce/article-pdf/21/17/8420/4126803O/ct5c00942.pdf by PEKING UNIV user on 04 November 2026

https://doi.org/10.1021/acs.jctc.5c00942
J. Chem. Theory Comput. 2025, 21, 8420−8433

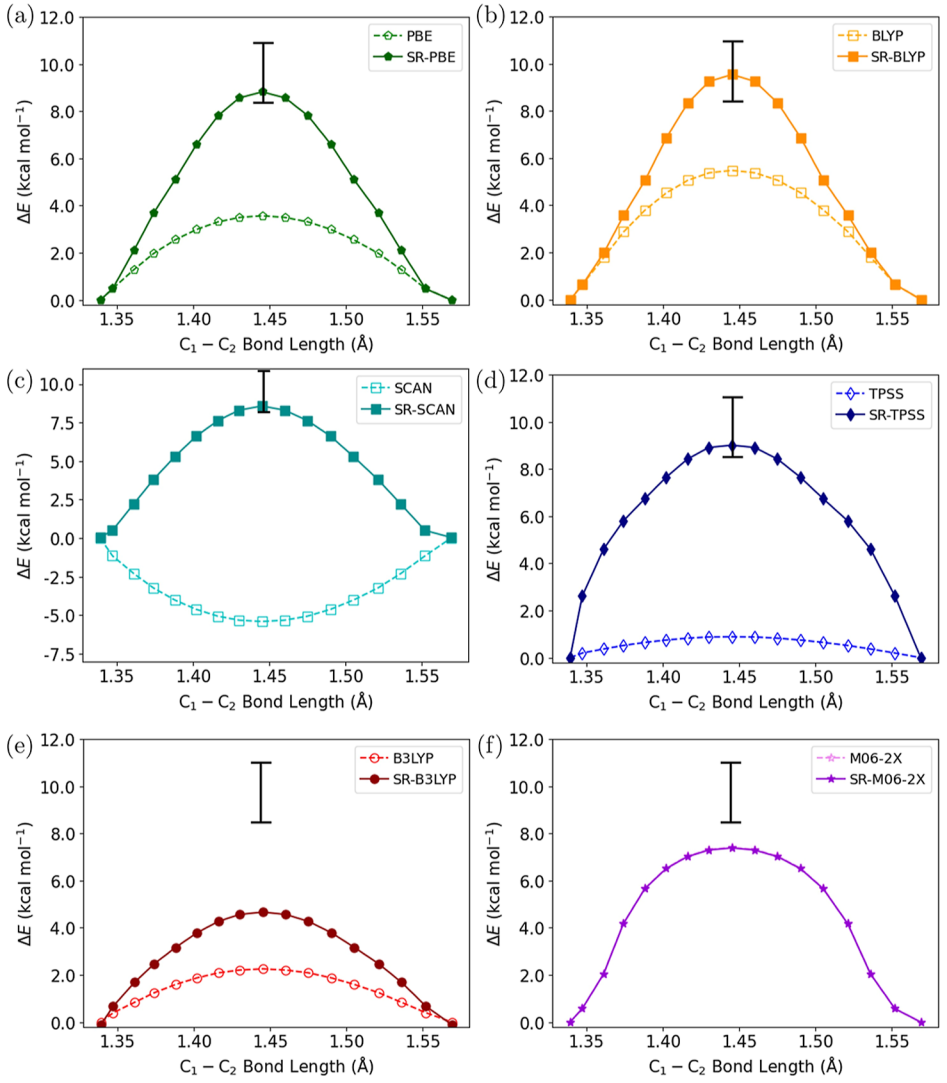

Figure 6. Mimimum energy paths generated from broken-symmetry DFT and SR-PDFT calculations using (a) PBE, (b) BLYP, (c) SCAN, (d) TPSS, (e) B3LYP, and (f) M06−2X as DFAs. Each panel includes a vertical black bar indicating the reference range for the barrier height calculated with multiconfigurational wave function methods, as extracted from Table 1.

Next, we quantitatively evaluated the improvement achieved by SR-PDFT upon broken-symmetry DFT results. The workflow of SR-PDFT involves two independent PDFT calculations carried out for each DFA: One sets $M_i = M_i^{\mathrm{DFA}}$ to reproduce the broken-symmetry DFT results, and the other enforces $M_i = M_i^{\mathrm{id}}$ to produce the regularized fragment spin-densities $\{n_{i\sigma}^{\mathrm{SR}}\}$. Those two sets of fragment spin-densities are then used to calculate the SR correction, i.e., the second term on the right-hand side of eq 17. In the case of H_2, broken-symmetry DFT only breaks the symmetries that are considered essential, so $M_i^{\mathrm{DFA}} = M_i^{\mathrm{id}}$ and the SR correction is zero. For CBD, the prefactor κ and the FOO-expressed nonadditive XC energy in eq 17 can be evaluated from the two above-mentioned sets of fragment spin-densities/populations. The other prefactor g, defined by eq 20, is determined by varying M_i for the transition state and finding the energy derivative with respect to it. For the automerization transition state, Table 2 lists all contributing components of the SR correction.

By computing the SR correction for all relevant structures, we obtain the MEPs presented in Figure 6. The reference range for the barrier height is indicated by the vertical black bar in each panel, and the original broken-symmetry DFT results are shown for comparison. Quantitative comparisons of barrier heights are available in Table 3. As we can see, SR-PDFT consistently increases the height of the reaction barrier compared to broken-symmetry DFT. Nonetheless, different DFAs exhibit varying degrees of correction, with some benefiting more from SR-PDFT than others. Panels (a) and (b) of Figure 6 show that SR-PDFT performs exceptionally well for GGAs and meta-GGAs. The SR correction was initially designed for PBE, so it brings about meaningful improvements upon the PBE broken-symmetry calculations across all structures along the MEP. By incorporating the function $g(s_{\mathrm{BLYP}})$, the correction also substantially improves the performance of BLYP. Both SR-PBE and SR-BLYP yield barrier heights that are in good agreement with those obtained from multireference wave function methods. From panels (c) and (d) of Figure 6, we know that SR-PDFT also works well with meta-GGAs. Although SCAN and TPSS significantly underestimate the barrier height in broken-symmetry DFT, they yield quantitatively accurate results upon the application of the SR correction. Problems arise when hybrid functionals

https://doi.org/10.1021/acs.jctc.5c00942
J. Chem. Theory Comput. 2025, 21, 8420−8433

Downloaded from pubs.acs.org/jctcce/article-pdf/21/17/8420/4126030/ct5c00942.pdf by PEKING UNIV user on 04 November 2026

Table 3. Automerization Barrier Height of CBD (in kcal mol^{-1}) from Broken-Symmetry DFT (E_b) and SR-PDFT (E_b^{SR})

DFA	E_b[a]	SR correction[b]	E_b^{SR}[a,c]
PBE	3.6	5.2	8.8
BLYP	5.5	4.1	9.6
SCAN	−5.4	14.0	8.6
TPSS	0.9	8.0	8.9
B3LYP	2.3	2.4	4.7
M06−2X	7.4	0.0	7.4
reference[d]			8.6−10.9

[a]The reported barrier heights are purely electronic and do not include zero-point vibrational energy corrections. [b]The SR correction refers to the second term on the right-hand side of eq 17. Values listed are for the autoemerization transition state. [c]The SR correction adds to the uncorrected barrier to yield the SR barrier height: $E_b^{SR} = E_b$ + SR Correction. [d]Same with those in Table 1, obtained from previous calculations.[37,38,45,46]

are used. Since the magnitudes of the XC energy obtained from B3LYP and M06−2X in broken-symmetry DFT are smaller than those from semilocal DFAs, the corresponding ΔE_{XC} magnitudes are consequently reduced as well, as indicated by Table 2. Furthermore, as evident from Figure 4c, the value of $g(s_{B3lYP})$ is significantly smaller compared to semilocal functionals, resulting in a relatively modest SR correction for the B3LYP functional. Consequently, as demonstrated in Figure 6e, while the SR correction raises the B3LYP barrier height, it does not achieve results that align with the reference values. SR-PDFT exhibits poorer performance when M06−2X is employed as the DFA. In contrast to the other five DFAs, the function g turns out to be a negative value for M06−2X, with its magnitude substantially smaller than those of other functionals. As a result, the effect of the SR correction becomes nearly negligible, leading to SR-PDFT yielding an MEP that is virtually indistinguishable from the broken-symmetry DFT result.

5. CONCLUDING REMARKS

A spin-density-functional regularization procedure has been integrated into the PDFT framework to correct the error introduced by broken-symmetry DFT in calculating the energy of singlet diradicals. We assessed the performance of SR-PDFT by applying it to the autoemerization transition state of CBD, a singlet diradical system that remains challenging even for state-of-the-art quantum chemical methods. Broken-symmetry DFT was found to overestimate the degree of local spin polarization in the transition state, leading to an underestimation of the autoemerization barrier height when calculations were performed with a variety of standard DFAs. Our results show that the SR correction significantly suppresses the error introduced by broken-symmetry DFT and yields quantitatively accurate MEPs for the autoemerization of CBD when employing semilocal functionals. In contrast to the previously developed overlap approximation (OA),[53,54,70] which is typically applied to spin-restricted DFT calculations, the SR correction provides an alternative approach to address strong electron correlation effects within the framework of broken-symmetry DFT. The method is tailored for open-shell singlet systems, particularly those with frontier orbitals occupied by spatially separated electrons (e.g., disjoint diradicals). SR-PDFT calculations can be efficiently performed using standard semilocal DFAs at negligible additional computational cost, making it a promising method for applications in condensed matter systems.

Nevertheless, SR-PDFT is far from perfect. First, the SR correction does not lead to an effective improvement on the total energy of the transition state when hybrid functionals are used in calculations. Also, the ideal fragment net spin populations $\{M_i^{id}\}$ are not determined through a rigorous distinction between essential and artificial symmetry breaking in broken-symmetry DFT. Rather, they are obtained by constructing a model function for each DFA. Finally, SR-PDFT provides only a simple correction to the total energy of molecules through postconvergence manipulations. Going forward, a crucial task is to establish a standard method for determining the ideal spin populations of molecules, especially for those with diradical characters between 0 and 1. More importantly, further research should explore how the SR correction affects other molecular properties that evolve alongside the energetic landscape, e.g., the forces applied to atoms derived from the PES, which could be accomplished by implementing the SR correction in a self-consistent manner.

■ ASSOCIATED CONTENT

Supporting Information

The Supporting Information is available free of charge at https://pubs.acs.org/doi/10.1021/acs.jctc.5c00942.

Details of ensemble setup in PDFT (Section S1); all necessary parameters used to generate the ideal spin populations for DFAs (Section S2); atomic coordinates of different CBD structures along the autoemerization MEP (Section S3) (PDF)

■ AUTHOR INFORMATION

Corresponding Authors

Adam Wasserman − *Department of Chemistry and Department of Physics and Astronomy, Purdue University, West Lafayette, Indiana 47907, United States;* orcid.org/0000-0002-8037-4453; Email: awasser@purdue.edu

Xin-Zheng Li − *State Key Laboratory for Artificial Microstructure and Mesoscopic Physics, Frontier Science Center for Nano-optoelectronics and School of Physics and Interdisciplinary Institute of Light-Element Quantum Materials, Research Center for Light-Element Advanced Materials, and Collaborative Innovation Center of Quantum Materials, Peking University, Beijing 100871, People's Republic of China; Peking University Yangtze Delta Institute of Optoelectronics, Nantong, Jiangsu 226010, People's Republic of China;* orcid.org/0000-0003-0316-4257; Email: xzli@pku.edu.cn

Authors

Yi Shi − *State Key Laboratory for Artificial Microstructure and Mesoscopic Physics, Frontier Science Center for Nano-optoelectronics and School of Physics, Peking University, Beijing 100871, People's Republic of China;* orcid.org/0009-0009-7918-5821

Yuming Shi − *Department of Materials Science and Engineering, Stanford University, Stanford, California 94305, United States*

Complete contact information is available at: https://pubs.acs.org/10.1021/acs.jctc.5c00942

Downloaded from pubs.acs.org/jctce/article-pdf/21/17/8420/4126803/ct5c00942.pdf by PEKING UNIV user on 04 November 2026

Notes

The authors declare no competing financial interest.

■ ACKNOWLEDGMENTS

Y.S. and X.-Z.L. are supported by the National Science Foundation of China under Grants No. 12234001, No. 12404257, No. 12474215, and No. 62321004, the National Basic Research Program of China under Grants No. 2021YFA1400500 and No. 2022YFA1403500. The computational resources are provided by the High-Performance Computing Platform of Peking University. A.W. was supported by NSF Award No. CHE-2306011.

■ REFERENCES

(1) Blundell, S. J. Molecular magnets. *Contemp. Phys.* **2007**, *48*, 275−290.
(2) Abdurahman, A.; Shen, L.; Wang, J.; Niu, M.; Li, P.; Peng, Q.; Wang, J.; Lu, G. A highly efficient open-shell singlet luminescent diradical with strong magnetoluminescence properties. *Light:Sci. Appl.* **2023**, *12*, 272.
(3) Hudson, J. M.; Hele, T. J. H.; Evans, E. W. Efficient light-emitting diodes from organic radicals with doublet emission. *J. Appl. Phys.* **2021**, *129*, 180901.
(4) Castro, C.; Karney, W. L. Heavy-Atom Tunneling in Organic Reactions. *Angew. Chem., Int. Ed.* **2020**, *59*, 8355−8366.
(5) Guo, W.; Robinson, E. E.; Thomson, R. J.; Tantillo, D. J. Heavy Atom Quantum Mechanical Tunneling in Total Synthesis. *Org. Lett.* **2024**, *26*, 4606−4609.
(6) Qiu, G.; Schreiner, P. R. The Intrinsic Barrier Width and Its Role in Chemical Reactivity. *ACS Cent. Sci.* **2023**, *9*, 2129−2137.
(7) Michel, C. S.; Lampkin, P. P.; Shezaf, J. Z.; Moll, J. F.; Castro, C.; Karney, W. L. Tunneling by 16 Carbons: Planar Bond Shifting in [16]Annulene. *J. Am. Chem. Soc.* **2019**, *141*, 5286−5293.
(8) Dewar, M. J.; Merz, K. M.; Stewart, J. J. Tunneling Dynamics of Cyclobutadiene. *J. Am. Chem. Soc.* **1984**, *106*, 4040−4041.
(9) Čársky, P.; Bartlett, R. J.; Fitzgerald, G.; Noga, J.; Špirko, V. Ab initio calculations on the energy of activation and tunneling in the automerization of cyclobutadiene. *J. Chem. Phys.* **1988**, *89*, 3008−3015.
(10) Carpenter, B. K. Heavy-atom tunneling as the dominant pathway in a solution-phase reaction? Bond shift in antiaromatic annulenes. *J. Am. Chem. Soc.* **1983**, *105*, 1700−1701.
(11) Schoonmaker, R.; Lancaster, T.; Clark, S. J. Quantum mechanical tunneling in the automerization of cyclobutadiene. *J. Chem. Phys.* **2018**, *148*, 104109.
(12) Stuyver, T.; Chen, B.; Zeng, T.; Geerlings, P.; De Proft, F.; Hoffmann, R. Do Diradicals Behave like Radicals? *Chem. Rev.* **2019**, *119*, 11291−11351.
(13) Hinz, A.; Bresien, J.; Breher, F.; Schulz, A. Heteroatom-Based Diradical(oid)s. *Chem. Rev.* **2023**, *123*, 10468−10526.
(14) Hegarty, D.; Robb, M. A. Application of unitary group methods to configuration interaction calculations. *Mol. Phys.* **1979**, *38*, 1795−1812.
(15) Eade, R. H. A.; Robb, M. A. Direct minimization in mc scf theory. the quasi-newton method. *Chem. Phys. Lett.* **1981**, *83*, 362−368.
(16) Siegbahn, P. E. M. A new direct CI method for large CI expansions in a small orbital space. *Chem. Phys. Lett.* **1984**, *109*, 417−423.
(17) Andersson, K.; Malmqvist, P. A.; Roos, B. O.; Sadlej, A. J.; Wolinski, K. Second-order perturbation theory with a CASSCF reference function. *J. Phys. Chem.* **1990**, *94*, 5483−5488.
(18) Andersson, K.; Malmqvist, P.; Roos, B. O. Second-order perturbation theory with a complete active space self-consistent field reference function. *J. Chem. Phys.* **1992**, *96*, 1218−1226.
(19) Meissner, L. Size-consistency corrections for configuration interaction calculations. *Chem. Phys. Lett.* **1988**, *146*, 204−210.
(20) Harju, A.; Räsänen, E.; Saarikoski, H.; Puska, M. J.; Nieminen, R. M.; Niemelä, K. Broken symmetry in density-functional theory: Analysis and cure. *Phys. Rev. B* **2004**, *69*, 153101.
(21) Jacob, C. R.; Reiher, M. Spin in density-functional theory. *Int. J. Quantum Chem.* **2012**, *112*, 3661−3684.
(22) Cohen, A. J.; Mori-Sánchez, P.; Yang, W. Challenges for Density Functional Theory. *Chem. Rev.* **2012**, *112*, 289−320.
(23) Andrews, J. S.; Jayatilaka, D.; Bone, R. G. A.; Handy, N. C.; Amos, R. D. Spin contamination in single-determinant wavefunctions. *Chem. Phys. Lett.* **1991**, *183*, 423−431.
(24) Baker, J.; Scheiner, A.; Andzelm, J. Spin contamination in density functional theory. *Chem. Phys. Lett.* **1993**, *216*, 380−388.
(25) Gräfenstein, J.; Cremer, D. Can density functional theory describe multi-reference systems? Investigation of carbenes and organic biradicals. *Phys. Chem. Chem. Phys.* **2000**, *2*, 2091−2103.
(26) Gräfenstein, J.; Kraka, E.; Filatov, M.; Cremer, D. Can Unrestricted Density-Functional Theory Describe Open Shell Singlet Biradicals? *Int. J. Mol. Sci.* **2002**, *3*, 360−394.
(27) Perdew, J. P.; Ruzsinszky, A.; Sun, J.; Nepal, N. K.; Kaplan, A. D. Interpretations of ground-state symmetry breaking and strong correlation in wavefunction and density functional theories. *Proc. Natl. Acad. Sci. U.S.A.* **2021**, *118*, No. e2017850118.
(28) Caballol, R.; Castell, O.; Illas, F.; de P R Moreira, I.; Malrieu, J. P. Remarks on the Proper Use of the Broken Symmetry Approach to Magnetic Coupling. *J. Phys. Chem. A* **1997**, *101*, 7860−7866.
(29) Yamaguchi, K.; Jensen, F.; Dorigo, A.; Houk, K. N. A spin correction procedure for unrestricted Hartree-Fock and Møller-Plesset wavefunctions for singlet diradicals and polyradicals. *Chem. Phys. Lett.* **1988**, *149*, 537−542.
(30) Ess, D. H.; Johnson, E. R.; Hu, X.; Yang, W. Singlet-triplet energy gaps for diradicals from fractional-spin density-functional theory. *J. Phys. Chem. A* **2011**, *115*, 76−83.
(31) Peng, D.; Hu, X.; Devarajan, D.; Ess, D. H.; Johnson, E. R.; Yang, W. Variational fractional-spin density-functional theory for diradicals. *J. Chem. Phys.* **2012**, *137*, 114112.
(32) Voter, A. F.; Goddard, W. A. The generalized resonating valence bond description of cyclobutadiene. *J. Am. Chem. Soc.* **1986**, *108*, 2830−2837.
(33) Borden, W. T.; Davidson, E. R. Theoretical studies of diradicals containing four.pi. electrons. *Acc. Chem. Res.* **1981**, *14*, 69−76.
(34) Monino, E.; Boggio-Pasqua, M.; Scemama, A.; Jacquemin, D.; Loos, P. F. Reference Energies for Cyclobutadiene: Automerization and Excited States. *J. Phys. Chem. A* **2022**, *126*, 4664−4679.
(35) David, G.; Ben Amor, N.; Zeng, T.; Suaud, N.; Trinquier, G.; Malrieu, J.-P. Difficulty of the evaluation of the barrier height of an open-shell transition state between closed shell minima: The case of small C_{4n} rings. *J. Chem. Phys.* **2022**, *156*, 224104.
(36) Yang, Y.; Peng, D.; Davidson, E. R.; Yang, W. Singlet-triplet energy gaps for diradicals from particle-particle random phase approximation. *J. Phys. Chem. A* **2015**, *119*, 4923−4932.
(37) Eckert-Maksić, M.; Vazdar, M.; Barbatti, M.; Lischka, H.; Maksić, Z. B. Automerization reaction of cyclobutadiene and its barrier height: An ab initio benchmark multireference average-quadratic coupled cluster study. *J. Chem. Phys.* **2006**, *125*, 064310.
(38) Shen, J.; Piecuch, P. Combining active-space coupled-cluster methods with moment energy corrections via the CC(P;Q) methodology, with benchmark calculations for biradical transition states. *J. Chem. Phys.* **2012**, *136*, 144104.
(39) Demel, O.; Pittner, J. Multireference Brillouin-Wigner coupled clusters method with noniterative perturbative connected triples. *J. Chem. Phys.* **2006**, *124*, 144112.
(40) Demel, O.; Shamasundar, K. R.; Kong, L.; Nooijen, M. Application of double ionization state-specific equation of motion coupled cluster method to organic diradicals. *J. Phys. Chem. A* **2008**, *112*, 11895−11902.
(41) Balková, A.; Bartlett, R. J. A multireference coupled-cluster study of the ground state and lowest excited states of cyclobutadiene. *J. Chem. Phys.* **1994**, *101*, 8972−8987.

Downloaded from pubs.acs.org/jctcce/article-pdf/21/17/8420/4126030/ct5c00942.pdf by PEKING UNIV user on 04 November 2026

https://doi.org/10.1021/acs.jctc.5c00942
J. Chem. Theory Comput. 2025, 21, 8420−8433

(42) Lyakh, D. I.; Lotrich, V. F.; Bartlett, R. J. The 'tailored' CCSD(T) description of the automerization of cyclobutadiene. *Chem. Phys. Lett.* **2011**, *501*, 166−171.
(43) Levchenko, S. V.; Krylov, A. I. Equation-of-motion spin-flip coupled-cluster model with single and double substitutions: Theory and application to cyclobutadiene. *J. Chem. Phys.* **2004**, *120*, 175−185.
(44) Bhaskaran-Nair, K.; Demel, O.; Pittner, J. Multireference state-specific Mukherjee's coupled cluster method with noniterative triexcitations. *J. Chem. Phys.* **2008**, *129*, 184105.
(45) Li, X.; Paldus, J. Accounting for the exact degeneracy and quasidegeneracy in the automerization of cyclobutadiene via multi-reference coupled-cluster methods. *J. Chem. Phys.* **2009**, *131*, 114103.
(46) Zhang, T.; Li, C.; Evangelista, F. A. Improving the Efficiency of the Multireference Driven Similarity Renormalization Group via Sequential Transformation, Density Fitting, and the Noninteracting Virtual Orbital Approximation. *J. Chem. Theory Comput.* **2019**, *15*, 4399−4414.
(47) Deustua, J. E.; Shen, J.; Piecuch, P. High-level coupled-cluster energetics by Monte Carlo sampling and moment expansions: Further details and comparisons. *J. Chem. Phys.* **2021**, *154*, 124103.
(48) Saito, T.; Nishihara, S.; Yamanaka, S.; Kitagawa, Y.; Kawakami, T.; Yamada, S.; Isobe, H.; Okumura, M.; Yamaguchi, K. Symmetry and broken symmetry in molecular orbital description of unstable molecules IV: Comparison between single- and multi-reference computational results for antiaromtic molecules. *Theor. Chem. Acc.* **2011**, *130*, 749−763.
(49) Lee, J.; Head-Gordon, M. Distinguishing artificial and essential symmetry breaking in a single determinant: Approach and application to the C_{60}, C_{36}, and C_{20} fullerenes. *Phys. Chem. Chem. Phys.* **2019**, *21*, 4763−4778.
(50) Lee, J.; Head-Gordon, M. Two single-reference approaches to singlet biradicaloid problems: Complex, restricted orbitals and approximate spin-projection combined with regularized orbital-optimized Møller-Plesset perturbation theory. *J. Chem. Phys.* **2019**, *150*, 244106.
(51) Lee, J.; Malone, F. D.; Morales, M. A. Utilizing Essential Symmetry Breaking in Auxiliary-Field Quantum Monte Carlo: Application to the Spin Gaps of the C36 Fullerene and an Iron Porphyrin Model Complex. *J. Chem. Theory Comput.* **2020**, *16*, 3019−3027.
(52) Elliott, P.; Burke, K.; Cohen, M. H.; Wasserman, A. Partition density-functional theory. *Phys. Rev. A* **2010**, *82*, 024501.
(53) Shi, Y.; Shi, Y.; Wasserman, A. Strong electron correlation from partition density functional theory. *J. Chem. Phys.* **2023**, *159*, 224108.
(54) Shi, Y.; Shi, Y.; Wasserman, A. Stretching Bonds without Breaking Symmetries in Density Functional Theory. *J. Phys. Chem. Lett.* **2024**, *15*, 826−833.
(55) Kollmar, H.; Staemmler, V. Violation of Hund's rule by spin polarization in molecules. *Theor. Chim. Acta* **1978**, *48*, 223−239.
(56) Perdew, J. P.; Burke, K.; Ernzerhof, M. Generalized Gradient Approximation Made Simple. *Phys. Rev. Lett.* **1996**, *77*, 3865−3868.
(57) Coulson, C. A.; Fischer, I. XXXIV Notes on the molecular orbital treatment of the hydrogen molecule. *London, Edinburgh Dublin Phil. Mag. J. Sci.* **1949**, *40*, 386−393.
(58) Nakano, M.; Champagne, B. Diradical character dependences of the first and second hyperpolarizabilities of asymmetric open-shell singlet systems. *J. Chem. Phys.* **2013**, *138*, 244306.
(59) Elliott, P.; Cohen, M. H.; Wasserman, A.; Burke, K. Density Functional Partition Theory with Fractional Occupations. *J. Chem. Theory Comput.* **2009**, *5*, 827−833.
(60) Perdew, J. P.; Parr, R. G.; Levy, M.; Balduz, J. L. Density-Functional Theory for Fractional Particle Number: Derivative Discontinuities of the Energy. *Phys. Rev. Lett.* **1982**, *49*, 1691−1694.
(61) Chai, J.-D. Density functional theory with fractional orbital occupations. *J. Chem. Phys.* **2012**, *136*, 154104.
(62) Zhang, K.; Wasserman, A. Split electrons in partition density functional theory. *J. Chem. Phys.* **2022**, *156*, 224113.
(63) Jiang, K.; Nafziger, J.; Wasserman, A. Constructing a non-additive non-interacting kinetic energy functional approximation for covalent bonds from exact conditions. *J. Chem. Phys.* **2018**, *149*, 164112.
(64) Sun, Q.; Berkelbach, T. C.; Blunt, N. S.; Booth, G. H.; Guo, S.; Li, Z.; Liu, J.; McClain, J. D.; Sayfutyarova, E. R.; Sharma, S.; Wouters, S.; Chan, G. K.-L. PySCF: the Python-based simulations of chemistry framework. *Wiley Interdiscip. Rev. Comput. Mol. Sci.* **2018**, *8*, No. e1340.
(65) Sun, Q. Libcint: An efficient general integral library for Gaussian basis functions. *J. Comput. Chem.* **2015**, *36*, 1664−1671.
(66) Sun, Q.; Zhang, X.; Banerjee, S.; Bao, P.; Barbry, M.; Blunt, N. S.; Bogdanov, N. A.; Booth, G. H.; Chen, J.; Cui, Z. H.; et al. Recent developments in the PySCF program package. *J. Chem. Phys.* **2020**, *153*, 024109.
(67) Dunning, T. H., Jr Gaussian basis sets for use in correlated molecular calculations. I. The atoms boron through neon and hydrogen. *J. Chem. Phys.* **1989**, *90*, 1007−1023.
(68) Frisch, M. J.; et al. *Gaussian 16*. Revision C.02; Gaussian Inc: Wallingford CT, 2016.
(69) Perdew, J. P.; Schmidt, K. Jacob's ladder of density functional approximations for the exchange-correlation energy. *AIP Conf. Proc.* **2001**, *577*, 1−20.
(70) Nafziger, J.; Wasserman, A. Fragment-based treatment of delocalization and static correlation errors in density-functional theory. *J. Chem. Phys.* **2015**, *143*, 234105.

Downloaded from pubs.acs.org/jctcce/article-pdf/21/17/8420/4126030/ct5c00942.pdf by PEKING UNIV user on 04 November 2026

https://doi.org/10.1021/acs.jctc.5c00942
J. Chem. Theory Comput. 2025, 21, 8420−8433